Research Article

Repairing whole facial nerve defects with xenogeneic acellular nerve grafts in rhesus monkeys

https://doi.org/10.4103/1673-5374.324853

Date of submission: January 27, 2021

Date of decision: January 29, 2021

Date of acceptance: March 30, 2021

Date of web publication: September 17, 2021

Guo-Chen Zhu[1, 2, *], Da-Jiang Xiao[1, 2, *], Bi-Wen Zhu[3], Yan Xiao[4]

Graphical Abstract *Application of the xenogeneic acellular nerve grafts to bridge whole facial nerve defects may be a suitable choice, if no other method is available*

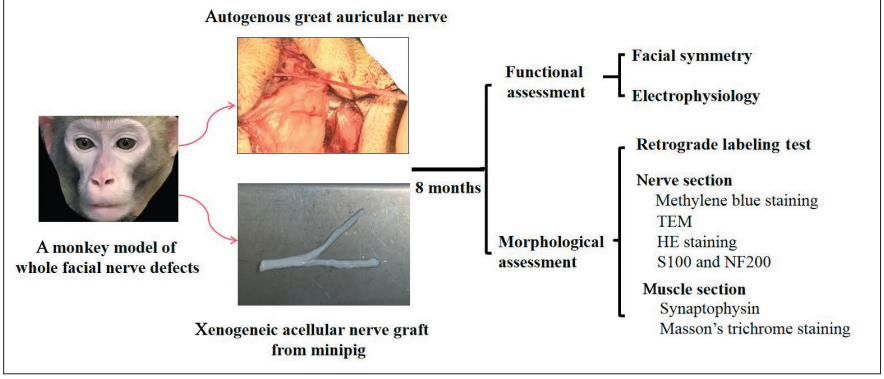

Abstract

Acellular nerve allografts conducted via chemical extraction have achieved satisfactory results in bridging whole facial nerve defects clinically, both in terms of branching a single trunk and in connecting multiple branches of an extratemporal segment. However, in the clinical treatment of facial nerve defects, allogeneic donors are limited. In this experiment, we exposed the left trunk and multiple branches of the extratemporal segment in six rhesus monkeys and dissected a gap of 25 mm to construct a monkey model of a whole left nerve defect. Six monkeys were randomly assigned to an autograft group or a xenogeneic acellular nerve graft group. In the autograft group, the 25-mm whole facial nerve defect was immediately bridged using an autogenous ipsilateral great auricular nerve, and in the xenogeneic acellular nerve graft group, this was done using a xenogeneic acellular nerve graft with trunk-branches. Examinations of facial symmetry, nerve-muscle electrophysiology, retrograde transport of labeled neuronal tracers, and morphology of the regenerated nerve and target muscle at 8 months postoperatively showed that the faces of the monkey appeared to be symmetrical in the static state and slightly asymmetrical during facial movement, and that they could actively close their eyelids completely. The degree of recovery from facial paralysis reached House-Brackmann grade II in both groups. Compound muscle action potentials were recorded and orbicularis oris muscles responded to electro-stimuli on the surgical side in each monkey. FluoroGold-labeled neurons could be detected in the facial nuclei on the injured side. Immunohistochemical staining showed abundant neurofilament-200-positive axons and soluble protein-100-positive Schwann cells in the regenerated nerves. A large number of mid-graft myelinated axons were observed via methylene blue staining and a transmission electron microscope. Taken together, our data indicate that xenogeneic acellular nerve grafts from minipigs are safe and effective for repairing whole facial nerve defects in rhesus monkeys, with an effect similar to that of autologous nerve transplantation. Thus, a xenogeneic acellular nerve graft may be a suitable choice for bridging a whole facial nerve defect if no other method is available. The study was approved by the Laboratory Animal Management Committee and the Ethics Review Committee of the Affiliated Wuxi No. 2 People's Hospital of Nanjing Medical University, China (approval No. 2018-D-1) on March 15, 2018.

Key Words: acellular nerve; compound muscle action potentials; facial nerve defect; facial symmetry; monkey; nerve graft; nerve regeneration; retrograde labeling test; synaptophysin; xenogeneic

Chinese Library Classification No. R459.9; R363; R364

Introduction

Facial nerve defects involving the extratemporal common facial trunk and its bifurcation or trifurcation have been described by Hu et al. (2010) as whole facial nerve defects. Whole facial nerve defect can lead to paralysis of all of the facial mimetic muscles, leading to impaired eyelid closure and

[1]Department of Otorhinolaryngology-Head and Neck Surgery, Affiliated Wuxi No. 2 People's Hospital of Nanjing Medical University, Wuxi, Jiangsu Province, China; [2]Department of Otorhinolaryngology-Head and Neck Surgery, Affiliated Wuxi Clinical College of Nantong University, Wuxi, Jiangsu Province, China; [3]College of Animal Science & Technology, Zhongkai University of Agriculture and Engineering, Guangzhou, Guangdong Province, China; [4]Department of Pathology, Affiliated Wuxi No.2 People's Hospital of Nanjing Medical University, Wuxi, Jiangsu Province, China

*Correspondence to: Guo-Chen Zhu, MD, zgc2003doctor@njmu.edu.cn; Da-Jiang Xiao, dajiang2125@163.com.

https://orcid.org/0000-0003-4814-1550 (Guo-Chen Zhu); https://orcid.org/0000-0002-8085-9274 (Da-Jiang Xiao)

Funding: *This work was financially supported by the National Natural Science Foundation of China, No. 81770990 (to GCZ); Jiangsu Provincial Key Research and Development Program of China, No. BE2018628 (to GCZ); Six Talent Peaks Project in Jiangsu Province of China, No. 2019-WSW-141 (to GCZ); Major Medicine Projects of Wuxi Health Commission of Jiangsu, China, No. Z201802 (to DJX); Precision Medicine Projects of Wuxi Health Commission of Jiangsu, China, No. J202002 (to GCZ).*

How to cite this article: *Zhu GC, Xiao DJ, Zhu BW, Xiao Y (2022) Repairing whole facial nerve defects with xenogeneic acellular nerve grafts in rhesus monkeys. Neural Regen Res 17(5):1131-1137.*

oral commissure elevation, as well as deviation of the nasal bridge and lower lip. To date, autologous nerve grafting, such as that of the great auricular nerve (Altafulla et al., 2019; Li et al., 2021) or sural nerve (Lee et al., 2015; Yi et al., 2020; Li et al., 2021), remains the gold standard of surgical treatment for bridging such facial nerve defects, although it is sometimes necessary to split the grafts into several strands (Prasad et al., 2018), choose multiple autologous nerves (Beutner and Grosheva et al., 2019), or create a free vascularized nerve flap (Mangialardi et al., 2021). However, there are some disadvantages of autografting in this area, such as the shortage of appropriate graft sites (trunk-branch type), donor site loss of function, and donor-recipient structural mismatch. Hence, there is increasing demand for alternative scaffolds. Although synthetic biomaterials, such as chitosan, silicone, polyglycolic acid, and poly (lactic-co-glycolic acid) (Wu et al., 2018; Neubrech et al., 2018; Niimi et al., 2019; Dolkhani et al., 2020), may guide nerve regeneration, it is difficult to direct them to form in the shape of trunk-branches (in terms of stem and branch diameters, lengths, and angles) that resemble the extratemporal facial nerve. Hence, this approach can only be applied for repairing a nerve defect in a single branch model.

In 1998, Sondell et al. reported that decellularizing peripheral nerves via chemical extraction could effectively eliminate the main immunogenic substances such as Schwann cells and myelin sheath and retain the main components of the nerve tissue extracellular matrix. Like autologous nerves, such allogenic decellularized scaffolds could guide the migration of host Schwann cells and support the movement of regenerated axons towards the target tissue without signs of immune rejection or excessive inflammation (Pan et al., 2019; Qiao et al., 2019; Yu et al., 2020). In recent years, allogenic acellular nerve grafts using chemical extraction have been used successfully to bridge peripheral nerve defects (Zhu et al., 2017), especially plexiform nerve defects, such as those involving the whole facial nerve (Hu et al., 2016) and brachial plexus (Li et al., 2019).

However, in clinical treatment, allogenic donors are restricted for patients with a whole facial nerve defect. Recently, various types of acellular matrix scaffolds have been produced from the mammalian extracellular matrix via chemical extraction (Li et al., 2020). Because they are easy to harvest and have low immunogenicity, these scaffolds have been used as xenografts in tissue engineering and regenerative medicine to reconstruct the human heart, gastrointestinal tract, pelvis, musculotendinous junction, and bladder (Holubec et al., 2015; Wong et al., 2016; Rutegård et al., 2019). However, few reports have described the repair of facial nerve defects, especially whole facial nerve defects, using xenogeneic acellular nerve grafts (XANGs) from a mammalian source (Zhu and Luo, 2014; Prest et al., 2018; Chai et al., 2019).

Although the shape, structure, and extracellular matrix of the peripheral nerves of the minipig are similar to those of humans (Lin et al., 2018), rigorous animal experiments are needed before they can be used clinically. However, Zhu and Luo (2014) have confirmed that the chemical extraction of XANGs is feasible for bridging facial nerve defects in rats, with promising results.

The large animal most suitable for making experimental models of whole facial nerve defect has not been determined (Wan et al., 2013; Gokce et al., 2016; Xue et al., 2016; Peng et al., 2018; Niimi et al., 2020). Beagle canines are docile and can collaborate with researchers to complete various experiments (Tsujimoto et al., 2017; Peng et al., 2018). However, their facial contours make it difficult to observe changes in facial expressions, particularly with respect to the symmetry of the bilateral oral commissure at rest and the movement of the mandible and lower lip while chewing or opening the mouth. Furthermore, the facial mimetic muscles of beagles are small and thin, making it difficult to perform electromyographical tests. Previous studies have indicated that minipigs and monkeys may be appropriate animal models for preclinical research regarding peripheral nerve injury and repair, although these models are associated with substantial costs and ethical circumspection (Satoda, 1987; Hontanilla et al., 2006; Lu et al., 2015; Aycart et al., 2015; Zhang et al., 2019; Milner et al., 2020). The buccal division of the facial nerve in minipigs is sufficiently thick, straight, and long that it can be used to bridge the defect of a single branch of the facial nerve. However, the common trunk of the extratemporal facial nerve and the origin of its four main divisions are located deep in the ramus mandibule, which cannot be observed via direct vision. Furthermore, the observation methods used to assess facial symmetry in minipigs require further development, as is the case with the techniques used for electrophysiological evaluation. Compared with minipigs, the anatomical characteristics of the monkey facial nerve share more similarities with humans, including the length, diameter, and types of divisions, although there are subtle differences among individuals (Satoda et al., 1987; Hontanilla et al., 2006). Therefore, monkeys may be more suitable than minipigs as an experimental model of facial nerve defects involving the common facial trunk and its main branches, and even the entire facial nerve. However, few investigations have reported on the application of nerve grafts for whole facial nerve defects in a monkey model. To address this in the present study, we sought to repair whole facial nerve defects in rhesus monkeys using XANGs from minipigs, and to observe the outcomes of nerve regeneration functionally and morphologically after the bridging operation.

Materials and Methods

Animals

The research subjects included six male rhesus monkeys and two male minipigs, provided by Suzhou Xishan ZhongKe Laboratory Animal Co., Ltd., China (license No. SYXK (Su) 2016-0042). The study was approved by the Laboratory Animal Management Committee and the Ethics Review Committee of the Affiliated Wuxi No. 2 People's Hospital of Nanjing Medical University, China (approval No. 2018-D-1) on March 15, 2018, which determined that the study design properly limited the number of animals used and employed an appropriate anesthetic protocol. All studies involving animals were reported in accordance with the Animal Research: Reporting *In Vivo* Experiments (ARRIVE) Guidelines. All animals were raised in single cages at room temperature at Suzhou Xishan Zhongke Pharmaceutical Research and Development Co., Ltd., and all surgical operations were performed by Guochen Zhu.

Preparation of XANGs

Segments of limb nerves suitable for bridging whole facial nerve defect in rhesus monkeys were harvested aseptically from two 4-month-old male minipigs, weighing 18–20 kg. The donor nerves included the brachial plexus, median nerve, radial nerve, common peroneal nerve, tibial nerve, and their branches (**Figure 1A**). The procedure for isolation of acellular nerve grafts (25 mm in length) was based on the method described by Sondell et al. (1998). Briefly, the nerves were immersed in distilled water for 7 hours, and then treated with 30 mL/L Triton X-100 (T9284, Sigma-Aldrich, St. Louis, MO, USA) in the absence of light for 12 hours. This was followed by 40 g/L sodium deoxycholate (D6750, Sigma-Aldrich) with agitation for 12 hours at room temperature. The extraction-procedure was repeated for two cycles. Finally, the extracted nerves were soaked in phosphate buffered saline solution (pH 7.2), sterilized via irradiation using the HFY-YC ^{60}Co irradiation

apparatus (Beijing Irradiation Source Science and Technology Development Co., Ltd., Beijing, China) for 12 hours at an intensity of 12 kilogray, and then stored at 4°C (**Figure 1B**).

Surgical procedure

Six monkeys weighing 5.45 ± 0.64 kg and aged 4.65 ± 0.46 years were randomly assigned into an autograft group (*n* = 3) and a XANG group (*n* = 3), with concealed allocation and a blinded assessor. All monkeys were anesthetized via a muscular injection of Zoletil™ 50 (Virbac Group, Nice, France). The left extratemporal facial nerve trunk and its main branches was exposed and dissected to create a 25-mm gap. In the autograft group (*n* = 3), this gap was immediately bridged using the autogenous ipsilateral great auricular nerve, which was folded into multiple strands. In the XANG group (*n* = 3), this was bridged using a trunk-multibranch type XANG according to the trunk-branches pattern of the whole facial nerve (**Figure 2A**). All anastomotic sites were sutured using 10-0 monofilament microsutures without tension. The operation was performed aseptically and assisted by an operation microscope (Olympus Optical Co., Tokyo, Japan). The opposite side of the body served as the control, enabling us to examine the effects of nerve resection and regeneration. After transplantation, all monkeys recovered for 8 months. All animals received injections of cefradine (North China Pharmaceutical Co., Ltd., Shijiazhuang, Hebei Province, China) intramuscularly for 5 days postoperatively, and did not receive any immunosuppressants during the perioperative period.

Functional and morphological assessment

Facial symmetry

Each monkey was photographed and videotaped using a digital camera (Canon LEGRIA HF G50, Tokyo, Japan) before injury, immediately after surgery, and at 1, 3, 5, and 8 months postoperatively. Changes in facial symmetry at rest were manually evaluated by surveying the α and β angle in each monkey at the different time points. As shown in **Figure 3**, in the resting state, line A connected the bilateral outer canthi; line B was the nasal bridge; line C was perpendicular to line A; and line D linked the bilateral oral commissure. The α angle was that intersected by line A and line B, while the β angle was defined as the angle between line C and line D. We calculated the value of the angle at the preoperative assessment minus that at the various postoperative time points. Additionally, we assessed the differences between the two groups in terms of facial symmetry, palpebral occlusion, and synkinetic movement during eye closure, opening of the mouth, and chewing (Socolovsky et al., 2016).

Electrophysiology

We performed electrophysiological evaluations of each monkey before dissection of the facial nerve and 8 months after the operation. Under general anesthesia (administered as mentioned above), a stimulating electrode was applied at the proximal end of the graft, and two bipolar needle electrodes were inserted into the orbicularis oris muscle of the ipsilateral lower lip. The compound muscle action potentials were recorded using a 16-channel electrophysiological instrument (MP150, BIOPAC System, Inc., Goleta, CA, USA). The measured parameters included the peak-to-peak amplitude and onset latency of the evoked compound muscle action potentials responses, and the data were analyzed using AcqKnowledge® 4.1 data acquisition and analysis tools (BIOPAC Systems, Inc., Goleta, CA, USA). To calculate the recovery ratios, we referred to the previous report by Zhu et al. (2014). Briefly, the onset latency recovery ratio of each monkey (%) was equal to the preoperative onset latency/postoperative onset latency of the left side × 100, and the peak-to-peak amplitude recovery ratio of each monkey (%) was equal to the postoperative peak-to-peak amplitude / preoperative peak-to-peak amplitude of the left side × 100.

Retrograde labeling test

We used the neural tracer FluoroGold as a retrograde marker of axonal regeneration of the facial nerve. Immediately after electrophysiological monitoring at 8 months postoperatively, 15 μL of 5% FluoroGold solution (F4040, US EVERBRIGHT®INC., Suzhou, Jiangsu Province, China) was injected at multiple points into the buccal division of the facial nerve, distal to the nerve graft. One week later, the monkeys received an overdose of anesthetic, and the upper part of the body was transcardially perfused with isotonic saline and 4% paraformaldehyde (pH 7.2) solution in turn. The pons was soaked in the same fixative for 36 hours and transferred to 30% sucrose at 4°C until sedimentation. Samples were sliced into 30-μm-thick frozen cross-sections using a Leica CM1950 freezing microtome (Leica Biosystems, Wetzlar, Hessen, Germany) at −20°C. Finally, the slices were examined using an inverted fluorescence microscope (Olympus IX51). The number of FluoroGold-labeled motor neurons was determined in accordance with a modified version of the method described by Fernandes et al. (2018).

Tissue analysis

After the animals were perfused at 8 months postoperatively, extratemporal facial nerve and facial mimetic musculature were harvested for histological examination. The mid-portions of the regenerative facial nerve trunk were harvested before perfusion and cut into 2 mm sections. The samples were immersed in 40 g/L neutral glutaraldehyde for 24 hours and then rinsed with 0.1 M sodium phosphate buffer at 4°C for 24 hours. The samples were post-fixed with 10 g/L osmium tetroxide at 4°C for 75 minutes and then rinsed with 0.1 M sodium phosphate buffer at 4°C for 40 minutes. After dehydrating the tissue using an acetone gradient, the specimens were embedded in Epoxy resin. Finally, semi-thin sections (1-μm thick) were stained with methylene blue to count the number of myelinated nerve fibers, while ultrathin sections (50-nm thick) were double stained with uranyl acetate and lead citrate to reveal the ultrastructure of the axons and myelin sheaths, viewed under a JEM-1230 transmission electron microscope (TEM, JEOL Ltd., Tokyo, Japan). Briefly, the mean values of the number of myelinated axons stained with methylene blue in each photo (×200, three photos per animal) were obtained from five different 10^4-μm^2 areas. All intact myelinated fibers were randomly selected from each TEM photomigraph (×1200, three photos per animal), and the mean value of the shortest distance and the longest distance passing through the center of each axon was regarded as the axon diameter. The main chemical reagents were purchased from Sigma-Aldrich (China) Biotechnology Co., Ltd. (Shanghai, China).

The mid-portions of the regenerative buccal branches of the facial nerve were fixed in 10% formalin, cut longitudinally or transversely into 4-μm-thick slices, and then stained with hematoxylin-eosin (Solarbio Life Sciences, Beijing, China). We then conducted immunohistochemistry to assess levels of soluble protein-100 (S100) and neurofilament 200, according to the MaxVision™3 kit (Maxim.Bio, Fuzhou, Fujian Province, China) manufacturer's protocol. The slides were deparaffinized in xylene, rehydrated in graded alcohol, and washed in tap water. Antigen retrieval was performed via treatment with ethylene diamine tetra-acetic acid (pH 8.0, Sangon Biotech Co., Ltd., Shanghai, China) for 15 minutes. Sections were incubated with mouse anti-human S100 monoclonal antibody (ab14849, Neomarkers, Fremont, CA, IL, USA) and mouse anti-human neurofilament 200 monoclonal antibody (MAB5262, Neomarkers) at a dilution of 1:100 for 1 hour at room temperature, respectively, and then washed three times with phosphate buffered saline-Tween 20 for 3 minutes.

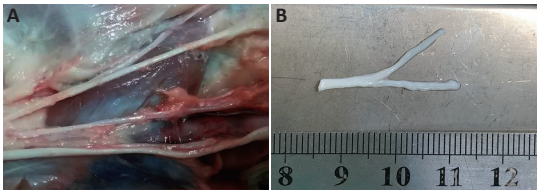

Figure 1 | **Acellular nerve graft from minipig.**
(A) Segment of fresh limb nerves; (B) acellular trunk-multibranch-type nerve graft.

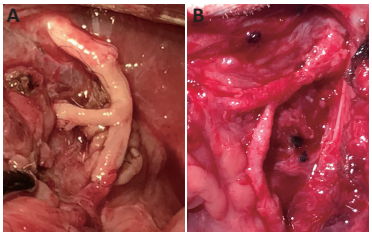

Figure 2 | **Gross view of the transplantation during the operation (A) and the regenerative nerves 8 months postoperatively (B) in the xenogeneic acellular nerve graft group.**

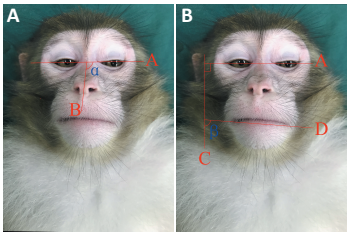

Figure 3 | **Observation and calculation of the α angle (left) and β angle (right) in the resting state (before nerve injury).**
Line A connected the bilateral outer canthi; line B was the nasal bridge; line C was perpendicular to line A; and line D linked the bilateral oral commissure. The α angle was that intersected by line A and line B, while the β angle was defined as the angle between line C and line D.

The sections were then incubated with HRP-Polymer anti-Mouse/Rabbit IgG for 30 minutes, and washed three times with phosphate buffered saline-Tween 20 for 3 minutes. The antigen-antibody complexes were visualized using diaminobenzidine with the same developing time, and counterstained with hematoxylin.

We conducted immunohistochemical staining for synaptophysin in the paraffin sections of the orbicularis oris muscle to observe the distribution of the presynaptic terminals in the neuromuscular junction (Rosko, 2018). We used the MaxVision^{TM}3 kit (Maxim.Bio) for immunohistochemistry as described above, and primary antibody synaptophysin (MS-1150-R1, Neomarkers) was diluted at a ratio of 1:100.

We conducted Masson's trichrome staining of the paraffin sections of the orbicularis oris muscle to assess morphological changes in muscle fibers. We followed the Masson's Trichrome Stain Kit (G1340; Solarbio Life Sciences) manufacturer's protocol. Sections were deparaffinized and hydrated, treated with Weigert's hematoxylin for 5 minutes to dye the cell nuclei, and then rinsed with distilled water. The sections were differentiated via application of 1% hydrochloric acid alcohol for 2 minutes and rinsed with tap water for 3 minutes. Afterwards, the tissues were stained using Masson complex solution (100 mL solution contains 0.7 g ponceau, 0.3 g acid fuchsin, 1 mL glacial acetic acid, and 99 mL distilled water) for 10 minutes, and rinsed with distilled water. The sections were differentiated via phosphomolybdic acid solution for 5 minutes, stained with 2% aniline blue dye solution for 5 minutes, and rinsed in 1% glacial acetic acid for 1 minute. Finally, the slices were observed under a light microscope after being dehydrated with 95% ethanol and anhydrous ethanol. After Masson's trichrome staining, the muscle fibers were labeled in red and the collagen fibers in blue.

Statistical analysis

Data were expressed as the mean ± SD. Statistical analysis was carried out using SPSS 24.0 Software (IBM, Armonk, NY, USA). After analyzing the homogeneity of variance and normal distribution, we used independent samples *t* tests to compare the means between the two groups and compared the difference between the preoperative angle and postoperative angle at different time points via a repeated measures analysis of variance. $P < 0.05$ was considered statistically significant.

Results

General status of the monkeys after the operation

All monkeys survived the operation and recovery process. The wounds of each monkey exhibited swelling within one week postoperatively, but none were infected, ulcerous, or cracked. At 8 months postoperatively, the XANGs were degraded and well integrated into the host tissue. The length of the graft segment had slightly decreased, and the proximal anastomosis was slightly coarser, but we observed neither dislocation of the grafts nor formation of neuroma in all monkeys (**Figure 2B**).

Recovery of facial symmetry in all groups

Before the operation, the degree of both the α angle and β angle at rest was an approximate right angle. These two angles generally increased after surgery, but this change was not statistically significant at 3 months ($P > 0.05$) (**Figure 4**). At 8 months postoperatively, each monkey appeared to have static facial symmetry, and the degree of these two angles at rest had recovered to an approximate right angle. As shown in **Table 1**, we found no statistically significant differences between the two groups in terms of the preoperative and postoperative angles at different time points ($P > 0.05$).

Table 1 | **Difference in the differential value between the preoperative angle (°) and the postoperative angle (°) at different time points and values in each group**

Group	1 mon	3 mon	5 mon	8 mon
Autograft				
Differential value of the α angle	5.03±0.57	4.92±0.50	2.90±0.26	0.97±0.21
Differential value of the β angle	20.27±2.00	19.05±1.95	6.47±0.31	0.97±0.47
XANG				
Differential value of the α angle	5.33±0.45	5.04±0.42	3.17±0.35	0.87±0.23
Differential value of the β angle	20.63±1.72	20.07±1.47	6.30±0.56	1.00±0.20

Data are expressed as the mean ± SD with three monkeys in each group.
XANG: Xenogeneic acellular nerve graft.

Immediately after the operation, each monkey could not completely close the left eyelid, and the oral commissure was clearly deviated. At 3 months postoperatively, there was partial recovery of the blink reflex and the oral commissure excursion on the paralyzed side. At 8 months after surgery, each monkey could actively close the eyelid completely. While opening the mouth or chewing fruit, mild oral commissure excursion and deviation of the mandible and lower lip was observed in both groups (**Figure 4**). There was one case of synkinesis in each group postoperatively.

Figure 4 | Postoperative facial photographs in the xenogeneic acellular nerve graft group.
(A) The oral commissure was clearly deviated at rest 1 month postoperatively. (B) The oral commissure was still deviated obviously at rest 3 months postoperatively. (C) The oral commissure was excursed and the mandible and lower lip were deviated while opening the mouth at 5 months postoperatively. (D) The oral commissure was mildly excursed and the mandible and lower lip were mildly deviated while opening the mouth wide at 8 months postoperatively.

Changes in electrophysiological parameters after the operation

Eight months postoperatively, compound muscle action potentials were recorded on the surgical side in each monkey. We found no significant differences between the two groups regarding onset latency recovery ratios or peak-to-peak amplitude recovery ratios ($P > 0.05$; **Table 2**).

Table 2 | Recovery ratios of compound muscle action potentials in each group at 8 months after surgery

	Peak amplitude		
Group	**Preoperation (mV)**	**Postoperation (mV)**	**Recovery ratios (%)**
Autograft	0.99±0.04	0.25±0.02	25.50±1.53
XANG	0.92±0.02	0.21±0.01	22.37±1.53
	Onset latency		
Group	**Preoperation (ms)**	**Postoperation (ms)**	**Recovery ratios (%)**
Autograft	1.68±0.25	2.91±0.16	52.47±3.65
XANG	1.43±0.10	2.83±0.14	50.52±3.49

Data are expressed as the mean ± SD ($n = 3$). XANG: Xenogeneic acellular nerve graft.

Changes in neurons in facial nerve tissue in each group via the retrograde labeling test

At 8 months after surgery, FluoroGold-labeled neurons with multipolar dendrites were seen in the lateral and intermediate regions of the facial nerve nuclei in both groups (**Figure 5A** and **B**). The number of labeled motor neurons was 75.22 ± 5.40 in the autograft group and 66.40 ± 10.71 in the XANG group ($P > 0.05$).

Histological changes in the regenerated facial nerve

At 8 months after surgery, the results of hematoxylin-eosin (**Figure 5C** and **D**), S100 immunohistochemical (**Figure 5E** and **F**), and neurofilament 200 immunohistochemical staining of the regenerated nerve in the two groups revealed abundant neovessels in the epineuria and among the perineuria and indicated that the regenerated nerve fiber bundles passed parallelly through the anastomotic sites.

The semi-thin sections and ultra-thin sections showed that the regenerated fibers were densely clustered with different sizes, and that the axons were widely distributed with an uneven density. Most of the myelin sheaths were arranged in the mature and uniform lamellar pattern, and the Schwann cells had perfect basement membranes (**Figure 5G** and **H**). There was no statistically significant difference in the number and diameter of myelinated axons or the myelin thickness between the two groups ($P > 0.05$; **Table 3**).

Table 3 | Regenerated nerve fibers in each group at 8 months after surgery

Group	Number of axons, fibers (/10^4 μm^2)	Axon diameter (μm)	Myelin thickness (μm)
Autograft	259.1±51.9	3.520±0.860	0.605±0.059
XANG	253.8±57.6	3.400±0.783	0.592±0.045

Data are expressed as the mean ± SD ($n = 3$). XANG: Xenogeneic acellular nerve graft.

Immunohistochemical staining of synaptophysin revealed that some motor endplates were reinnervated in the orbicularis oris muscle on the injured side in the two groups (**Figure 5I** and **J**). Masson staining of the orbicularis oris muscle indicated that the muscles had become smaller, with mild atrophy.

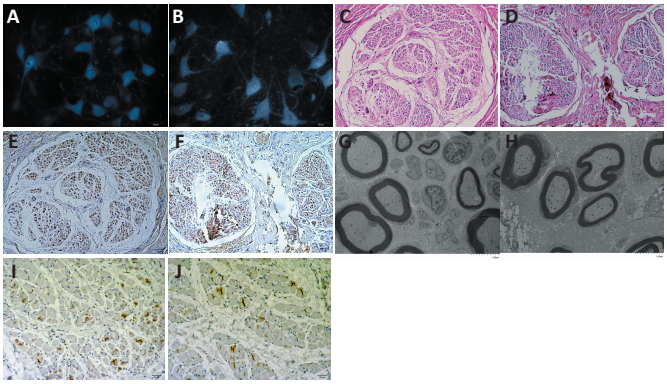

Figure 5 | Morphological assessment at 8 months postoperatively.
The Retrograde Labeling Test (original magnification, 400×; A, B) revealed FluoroGold-labeled neurons with multipolar dendrites in the facial nerve nuclei. Hematoxylin-eosin staining (original magnification, 200×; C, D) and S100 immunohistochemical staining (original magnification, 200×; E, F) showed the regenerated nerve fibers, and S100-positive Schwann cells and myelin sheaths were densely clustered, with different sizes, in the transverse section. Transmission electron micrographs (original magnification, 1200×; G, H) showed that most myelin sheaths were arranged in the mature and uniform lamellar pattern, and that the Schwann cells had perfect basement membranes. Synaptophysin immunohistochemical staining (original magnification, 200×; I, J) of the orbicularis oris muscle showed that some motor endplates were reinnervated in the muscle. (A, C, E, G, I) The autograft group; (B, D, F, H, J) the xenogeneic acellular nerve graft group.

Discussion

In the present study, the distribution pattern and number of branches in the extratemporal facial nerve within 20 mm distal to the stylomastoid foramen in adult rhesus monkey was one trunk with two or three branches, which is similar to that of human beings. Facial symmetry in the static state and active state (such as blinking, chewing, and opening the mouth) can easily be captured via photograph and videotape. Therefore, the whole facial nerve defect model in rhesus monkeys is suitable for preclinical study, especially for bridging defects with acellular nerve scaffolds (Hu et al., 2010).

Functional evaluation of graft materials in terms of facial nerve defect repair mainly depends on the functional recovery of paralyzed mimetic musculature. In a study by Wan et al. (2013), the α angle was used to measure changes in rat facial symmetry, and video recording was used to evaluate rat behaviors. Hadlock et al. (2012) and Oh et al. (2019) used FACEgram to calculate the smile excursion and the angle of oral commissure elevation on each side in facial palsy patients, and they used the ratio of the excursion distances on both sides to assess facial symmetry. We did not use the FACEgram program to measure facial movements in monkeys because they are aggressive towards humans and not able to sufficiently cooperate with researchers. In the present study, we calculated the α angle and the β angle for each monkey

from the pre-operation period to 8 months after surgery. We found that the variation in the α angle after surgery was similar to that in facial palsy patients, but not as dramatic as that in rats and rabbits (Gokce et al., 2016; Socolovsky et al., 2016). The degree of the β angle changed significantly after surgery in monkeys. Therefore, the authors propose that the β angle is a better prognostic parameter than the α angle for assessing monkey facial paralysis. At 8 months postoperatively, each monkey exhibited restored facial symmetry at rest, with only slight asymmetry during facial expressions. Furthermore, the monkeys could close the affected eyelid completely. There was one case of synkinesis in the XANG group and one case in the autograft group. Currently, preventing or alleviating facial synkinesis is one of the most important topics in facial nerve reconstruction (Mendez et al., 2018). Decreased synkinesis in the reinnervated facial nerve may be achieved via implantation of additional stem cells or brief electrical stimulation. However, studies focused on the repair of facial nerve defects have predominantly examined the single branch model of the extratemporal segment, and few reports have tested bridging of whole facial nerve defects. Thus, there are limited data regarding synkinesis (Hu et al., 2010, 2016). Both groups in the present study obtained a recovery score corresponding to House-Brackmann grade II (Wan et al., 2013; Thakar et al., 2018), which suggested that the facial functional outcome of the paralyzed side had recovered satisfactorily in each monkey. These results were similar to those described by Hontanilla et al. (2006).

Morphological evaluation of facial nerve regeneration can include the examination of motor neurons, regenerative nerves, and facial mimetic muscles (Ning and Xiong, 2011; Cao et al., 2021; Wu et al., 2021). Many studies have reported that FluoroGold can be transported to neuronal cell bodies through the axoplasm after being absorbed by axons (Hontanilla et al., 2006; Aycart et al., 2015; Lu et al., 2015). Compared with the horseradish peroxidase retrograde tracing method (Zhu and Luo, 2014; Wang et al., 2016), the FluoroGold procedure is simple: the frozen brain section can be directly observed using a fluorescence microscope after perfusion-fixation and complete immersion in sucrose solution. In this study, we observed labeled neurons in the inferior part of the pons after a microinjection of FluoroGold in each monkey. This procedure revealed the structural integrity of the neural pathways and recovery of axoplasm transport in the regenerated nerves. Additionally, our electrophysiological tests and tissue analyses revealed that the regenerated nerves passed through the scaffolds and reconstructed the neuromuscular junctions of the target muscles.

Limitations: Our function and morphology data showed that XANGs could repair whole facial nerve defects in primates, despite the small sample size. While our results would be more convincing if there were more animals enrolled in this experiment, studies involving large primate populations may raise ethical concerns. Further experimental studies in large animals are needed to address the length limitation of XANGs in repairing whole facial nerve defects, as well as the regeneration variance of different branches (Hu et al., 2007; Endo et al., 2019). In addition, future studies should examine the use of XANGs with autologous or allogeneic seed cells to bridge longer nerve gaps (Ee et al., 2017; Gu et al., 2019; Saez et al., 2019; Salehi et al., 2019). If these problems are addressed, this method could be applied to patients with large facial nerve defects.

Conclusion

Bridging whole facial nerve defects of the extratemporal segment with XANGs resulted in the functional recovery of paralyzed facial muscles in rhesus monkeys. Thus, XANGs may be a potential option for repairing whole facial nerve defects in humans when other methods are not available.

Acknowledgments: *The authors thank Mrs. Li Li and Mr. Minghao Wang from Department of Otorhinolaryngology-Head and Neck Surgery, Affiliated Wuxi Clinical College of Nantong University, Wuxi, Jiangsu, China for their excellent technical assistance.*

Author contributions: *Study conception, design, fundraising, administrative, technical or material support, and supervision: GCZ and DJX; experimental studies, data collection, and analysis and interpretation of the data, statistical expertise, writing the manuscript or providing critical revision of the manuscript for intellectual content: GCZ, BWZ and YX. All authors approved the final version of the manuscript.*

Conflicts of interest: *The authors declare that there are no conflicts of interest associated with this manuscript.*

Financial support: *This work was financially supported by the National Natural Science Foundation of China, No. 81770990 (to GCZ); Jiangsu Provincial Key Research and Development Program of China, No. BE2018628 (to GCZ); Six Talent Peaks Project in Jiangsu Province of China, No. 2019-WSW-141 (to GCZ); Major Medicine Projects of Wuxi Health Commission of Jiangsu, China, No. Z201802 (to DJX); Precision Medicine Projects of Wuxi Health Commission of Jiangsu, China, No. J202002 (to GCZ). The funding sources had no role in study conception and design, data analysis or interpretation, paper writing or deciding to submit this paper for publication.*

Institutional review board statement: *The study was endorsed by the Laboratory Animal Management Committee and the Ethics Review Committee of the Affiliated Wuxi No. 2 People's Hospital of Nanjing Medical University, China (approval No. 2018-D-1; Date: March 15, 2018). The experimental procedure followed the United States National Institutes of Health Guide for the Care and Use of Laboratory Animals (NIH Publication No. 85-23, revised 1996).*

Data sharing statement: *Datasets analyzed during the current study are available from the corresponding author on reasonable request.*

Plagiarism check: *Checked twice by iThenticate.*

Peer review: *Externally peer reviewed.*

References

Altafulla J, Iwanaga J, Lachkar S, Prickett J, Dupont G, Yilmaz E, Ishak B, Litvack Z, Tubbs RS (2019) The great auricular nerve: anatomical study with application to nerve grafting procedures. World Neurosurg 125:e403-407.

Aycart MA, Alhefzi M, Bueno E, Pomahac B (2015) Surgical anatomy of the whole facial nerve for enabling craniofacial and regenerative medicine translational research in swine. J Reconstr Microsurg 31:547-550.

Beutner D, Grosheva M (2019) Reconstruction of complex defects of the extracranial facial nerve: technique of "the trifurcation approach". Eur Arch Otorhinolaryngol 276:1793-1798.

Cao QQ, Li S, Lu Y, Wu D, Feng W, Shi Y, Zhang LP (2021) Transcriptome analysis of molecular mechanisms underlying facial nerve injury repair in rats. Neural Regen Res 16:2316-2323.

Chai HH, Chen MB, Chen GZ, Li ZZ, Xiu JG, Liu Y, Guo YW, Li SP (2019) Inhibitory effect of TGF-β gene modified human amniotic mesenchymal stem cells on rejection after xenotransplantation of peripheral nerves. Eur Rev Med Pharmacol Sci 23:3198-3205.

Dolkhani S, Najafpour A, Mohammadi R (2020) Fabrication and transplantation of chitosan-selenium biodegradable nanocomposite conduit on transected sciatic nerve: a novel study in rat model. Neurol Res 42:439-450.

Ee X, Yan Y, Hunter DA, Schellhardt L, Sakiyama-Elbert SE, Mackinnon SE, Wood MD (2017) Transgenic SCs expressing GDNF-IRES-DsRed impair nerve regeneration within acellular nerve allografts. Biotechnol Bioeng 114:2121-2130.

Endo T, Kadoya K, Suzuki Y, Kawamura D, Iwasaki N (2019) A novel experimental model to determine the axon-promoting effects of grafted cells after peripheral nerve injury. Front Cell Neurosci 13:280-291.

Fernandes M, Valente SG, Sabongi RG, Gomes Dos Santos JB, Leite VM, Ulrich H, Nery AA, da Silva Fernandes M (2018) Bone marrow-derived mesenchymal stem cells versus adipose-derived mesenchymal stem cells for peripheral nerve regeneration. Neural Regen Res 13:100-104.

Gokce Tulaci K, Tuzuner A, Karadas Emir H, Tatar İ, F Sargon M, Tulaci T, Karadavut Y, Erdal Samim E (2016) The effect of tacrolimus on facial nerve injury: histopathological findings in a rabbit model. Am J Otolarygol 37:393-397.

Hadlock TA, Urban LS (2012) Toward a universal, automated facial measurement tool in facial reanimation. Arch Facial Plast Surg 14:277-282.
Holubec T, Caliskan E, Bettex D, Maisano F (2015) Repair of post-infarction left ventricular free wall rupture using an extracellular matrix patch. Eur J Cardiothorac Surg 48:800-803.
Hontanilla B, Aubá C, Arcocha J, Gorría O (2006) Nerve regeneration through nerve autografts and cold preserved allografts using Tacrolimus (FK506) in a facial paralysis model: a topographical and neurophysiological study in monkeys. Neurosurgery 58:768-779.
Hu J, Zhu QT, Liu XL, Xu YB, Zhu JK (2007) Repair of extended peripheral nerve lesions in rhesus monkeys using acellular allogenic nerve grafts implanted with autologous mesenchymal stem cells. Exp Neurol 204:658-666.
Hu M, Xiao H, Niu Y, Liu H, Zhang L (2016) long-term follow-up of the repair of the multiple-branch facial nerve defect using acellular nerve allograft. J Oral Maxillofac Surg 74:218.e1-e11.
Hu M, Zhang L, Niu Y, Xiao H, Tang P, Wang Y (2010) Repair of whole rabbit facial nerve defects using facial nerve allografts. J Oral Maxillofac Surg 68:2196-2206.
Lee MC, Kim DH, Jeon YR, Rah DK, Lew DH, Choi EC, Lee WJ (2015) Functional outcomes of multiple sural nerve grafts for facial nerve defects after tumor-ablative surgery. Arch Plast Surg 42:461-468.
Li L, Fan Z, Wang H, Han Y (2021) Efficacy of surgical repair for the functional restoration of injured facial nerve. BMC Surg 21:32.
Li L, Yang J, Qin B, Wang H, Yang Y, Fang J, Chen G, Liu X, Tu Z, Gu L (2019) Analysis of human acellular nerve allograft combined with contralateral C7 nerve root transfer for restoration of shoulder abduction and elbow flexion in brachial plexus injury: a mean 4-year follow-up. J Neurosurg 132:1914-1924.
Li T, Sui Z, Matsuno A, Ten H, Oyama K, Ito A, Jiang H, Ren X, Javed R, Zhang L, Ao Q (2020) Fabrication and evaluation of a xenogeneic decellularized nerve-derived material: preclinical studies of a new strategy for nerve repair. Neurotherapeutics 17:356-370.
Lin T, Liu S, Chen S, Qiu S, Rao Z, Liu J, Zhu S, Yan L, Mao H, Zhu Q, Quan D, Liu X (2018) Hydrogel derived from porcine decellularized nerve tissue as a promising biomaterial for repairing peripheral nerve defects. Acta Biomater 73:326-338.
Lu C, Meng D, Cao J, Xiao Z, Cui Y, Fan J, Cui X, Chen B, Yao Y, Zhang Z, Ma J, Pan J, Dai J (2015) Collagen scaffolds combined with collagen-binding ciliary neurotrophic factor facilitate facial nerve repair in mini-pigs. J Biomed Mater Res A 103:1669-1676.
Mangialardi ML, Honart JF, Qassemyar Q, Guyon A, Li SS, Benmoussa N, Beldarida V, Temam S, Kolb F (2021) Reconstruction of extensive composite parotid region oncologic defects with immediate facial nerve reconstruction using a chimeric scapulodorsal vascularized nerve free flap. J Reconstr Microsurg 37:282-291.
Mendez A, Hopkins A, Biron VL, Seikaly H, Zhu LF, Côté DWJ (2018) Brief electrical stimulation and synkinesis after facial nerve crush injury: a randomized prospective animal study. J Otolaryngol Head Neck Surg 47:20-27.
Milner TD, Okhovat S, McGuigan M, Clement WA, Kunanandam T (2020) Feasibility of ovine and porcine models for simulation training in parotid surgery and facial nerve dissection. Eur Arch Otorhinolaryngol 277:1167-1175.
Neubrech F, Sauerbier M, Moll W, Seegmüller J, Heider S, Harhaus L, Bickert B, Kneser U, Kremer T (2018) Enhancing the outcome of traumatic sensory nerve lesions of the hand by additional use of a chitosan nerve tube in primary nerve repair: a randomized controlled bicentric trial. Plast Reconstr Surg 142:415-424.
Niimi Y, Matsumine H, Fukuda S, Salsbury JR, Niimi Y, Herndon DN, Prough DS, Enkhbaatar P (2020) Surgical anatomy of ovine facial and hypoglossal nerves for facial nerve reconstruction and regeneration research: an experimental study in sheep. Microsurgery 40:51-58.
Niimi Y, Matsumine H, Takeuchi Y, Hironobu O, Tsunoda S, Miyata M, Yamato M, Sakurai H (2019) A collagen-coated PGA conduit for interpositional-jump graft with end-to-side neurorrhaphy for treating facial nerve paralysis in rat. Microsurgery 39:70-80.
Ning LN, Xiong J (2011) Nerve tissue engineering scaffolds or heterologous nerve grafts in facial nerve defects. Zhongguo Zuzhi Gongcheng Yanjiu 15:3969-3971.
Oh TS, Kim HB, Choi JW, Jeong WS (2019) Facial reanimation with masseter nerve-innervated free gracilis muscle transfer in established facial palsy patients. Arch Plast Surg 46:122-128.
Pan D, Hunter DA, Schellhardt L, Jo S, Santosa KB, Larson EL, Fuchs AG, Snyder-Warwick AK, Mackinnon SE, Wood MD (2019) The accumulation of T cells within acellular nerve allografts is length-dependent and critical for nerve regeneration. Exp Neurol 318:216-231.
Peng Y, Li KY, Chen YF, Li XJ, Zhu S, Zhang ZY, Wang X, Duan LN, Luo ZJ, Du JJ, Wang JC (2018) Beagle sciatic nerve regeneration across a 30 mm defect bridged by chitosan/PGA artificial nerve grafts. Injury 49:1477-1484.
Prasad SC, Balasubramanian K, Piccirillo E, Taibah A, Russo A, He J, Sanna M (2018) Surgical technique and results of cable graft interpositioning of the facial nerve in lateral skull base surgeries: experience with 213 consecutive cases. J Neurosurg 128:631-638.
Prest TA, Yeager E, LoPresti ST, Zygelyte E, Martin MJ, Dong L, Gibson A, Olutoye OO, Brown BN, Cheetham J (2018) Nerve-specific, xenogeneic extracellular matrix hydrogel promotes recovery following peripheral nerve injury. J Biomed Mater Res A 106:450-459.
Qiao W, Lu L, Wu G, An X, Li D, Guo J (2019) DPSCs seeded in acellular nerve grafts processed by Myroilysin improve nerve regeneration. J Biomater Appl 33:819-833.
Rosko AJ, Kupfer RA, Oh SS, Haring CT, Feldman EL, Hogikyan ND (2018) Immunohistologic analysis of spontaneous recurrent laryngeal nerve reinnervation in a rat model. Laryngoscope 128:E117-122.
Rutegård M, Rutegård J, Haapamäki MM (2019) Multicentre, randomised trial comparing acellular porcine collagen implant versus gluteus maximus myocutaneous flap for reconstruction of the pelvic floor after extended abdominoperineal excision of rectum: study protocol for the Nordic Extended Abdominoperineal Excision (NEAPE) study. BMJ Open 9:e027255.
Saez DM, Sasaki RT, Martins DO, Chacur M, Kerkis I, da Silva MCP (2019) Rat facial nerve regeneration with human immature dental pulp stem cells. Cell Transplant 28:1573-1584.
Salehi MS, Borhani-Haghighi A, Pandamooz S, Safari A, Dargahi L, Dianatpour M, Tanideh N (2019) Dimethyl fumarate up-regulates expression of major neurotrophic factors in the epidermal neural crest stem cells. Tissue Cell 56:114-120.
Satoda T, Takahashi O, Tashiro T, Matsushima R, Uemura-Sumi M, Mizuno N (1987) Representation of the main branches of the facial nerve within the facial nucleus of the Japanese monkey (Macaca fuscata). Neurosci Lett 78:283-287.
Socolovsky M, Martins RS, di Masi G, Bonilla G, Siqueira M (2016) Treatment of complete facial palsy in adults: comparative study between direct hemihypoglossal-facial neurorrhaphy, hemihipoglossal-facial neurorrhaphy with grafts, and masseter to facial nerve transfer. Acta Neurochir (Wien) 158:945-957.
Sondell M, Lundborg G, Kanje M (1998) Regeneration of the rat sciatic nerve into allografts made acellular through chemical extraction. Brain Res 795:44-54.
Thakar A, Gupta MP, Srivastava A, Agrawal D, Kumar A (2018) Nonsurgical Treatment For Posttraumatic Complete Facial Nerve Paralysis. JAMA Otolaryngol Head Neck Surg 144:315-321.
Tsujimoto G, Sunada K, Nakamura T (2017) Effect of cervical sympathetic ganglionectomy on facial nerve reconstruction using polyglycolic acid-collagen tubes. Brain Res 1669:79-88.
Wan H, Zhang L, Blanchard S, Bigou S, Bohl D, Wang C, Liu S (2013) Combination of hypoglossal-facial nerve surgical reconstruction and neurotrophin-3 gene therapy for facial palsy. J Neurosurg 119:739-750.
Wang Y, Jia H, Li WY, Guan LX, Deng L, Liu YC, Liu GB (2016) Molecular examination of bone marrow stromal cells and chondroitinase ABC-assisted acellular nerve allograft for peripheral nerve regeneration. Exp Ther Med 12:1980-1992.
Wong ML, Wong JL, Vapniarsky N, Griffiths LG (2016) In vivo xenogeneic scaffold fate is determined by residual antigenicity and extracellular matrix preservation. Biomaterials 92:1-12.
Wu JJ, Lu YC, Zheng MX, Hua XY, Shan CL, Ding W, Xu JG (2021) Structural remodeling in related brain regions in patients with facial synkinesis. Neural Regen Res 16:2528-2533.
Wu W, Liu X, Zhou Z, Miller AL, Lu L (2018) Three-dimensional porous poly(propylene fumarate)-co-poly(lactic-co-glycolic acid) scaffolds for tissue engineering. J Biomed Mater Res A 106:2507-2517.
Xue C, Ren H, Zhu H, Gu X, Guo Q, Zhou Y, Huang J, Wang S, Zha G, Gu J, Yang Y, Gu Y, Gu X (2017) Bone marrow mesenchymal stem cell-derived acellular matrix-coated chitosan/silk scaffolds for neural tissue regeneration. J Mater Chem B 5:1246-1257.
Yi CR, Oh TM, Jeong WS, Choi JW, Oh TS (2020) Quantitative analysis of the impact of radiotherapy on facial nerve repair with sural nerve grafting after parotid gland surgery. J Craniomaxillofac Surg 48:724-732.
Yu T, Wen L, He J, Xu Y, Li T, Wang W, Ma Y, Ahmad MA, Tian X, Fan J, Wang X, Hagiwara H, Ao Q (2020) Fabrication and evaluation of an optimized acellular nerve allograft with multiple axial channels. Acta Biomater 115:235-249.
Zhang Z, Zhang C, Li Z, Zhang S, Liu J, Bai Y, Pan J, Zhang C (2019) Collagen/β-TCP nerve guidance conduits promote facial nerve regeneration in mini-swine and the underlying biological mechanism: a pilot in vivo study. J Biomed Mater Res B Appl Biomater 107:1122-1131.
Zhu G, Lou W (2014) Regeneration of facial nerve defects with xenogeneic acellular nerve grafts in a rat model. Head Neck 36:481-486.
Zhu S, Liu J, Zheng C, Gu L, Zhu Q, Xiang J, He B, Zhou X, Liu X (2017) Analysis of human acellular nerve allograft reconstruction of 64 injured nerves in the hand and upper extremity: a 3 year follow-up study. J Tissue Eng Regen Med 11:2314-2322.

C-Editor: Zhao M; S-Editors: Wang J, Li CH; L-Editors: Koke S, Hindle A, Qiu Y, Song LP; T-Editor: Jia Y